

Lithological and Si–O–S isotope geochemistry: constraints on the origin and genetic environment of the selenium (Se)-rich siliceous rocks in Enshi, Hubei Province, China

Caixia Feng¹ · Shen Liu¹ · Ian M. Coulson²

Received: 26 May 2020 / Revised: 30 September 2020 / Accepted: 2 November 2020 / Published online: 18 November 2020
© Science Press and Institute of Geochemistry, CAS and Springer-Verlag GmbH Germany, part of Springer Nature 2020

Abstract Se-rich black rock series of the Middle and Late Permian system is widely distributed in Enshi Prefecture with an exposed area of 850 km², among which the unique Yutangba black rock series independent selenium deposit with industrial mining significance in the world is produced. However, the source and metallogenic mechanisms of Se are still controversial. In general, terrestrial weathering and submarine hydrothermal processes are the main source end members of Si and Se, and the related siliceous rocks record the deposition process of Si and Se from different sources. The study of lithofacies and paleogeography shows that western Hubei belongs to the near east–west turn of the Yangzi platform in the Middle and Late Permian and becomes an inter-platform basin with nearly north–south direction. Therefore, the comparative study of the Yutangba deposit and the selenium-rich black rock series in the northern Shadi with high selenium content is expected to reveal the provenance evolution of the two sections in space, and further restrict the Se mineralization mechanism in the Enshi basin. From the element geochemistry study, the black rock series in two study areas may have formed in a transitional position of either the continental margin or continental slope, in the process of sedimentary, more terrigenous clastic materials entered. They are rich in lithophile elements V and Cr. $\delta\text{U} > 1.0$, U/Th and V/(V + Ni) ratio indicate that the Se-rich strata

of black rock series in the Enshi areas occurred in an anoxic reducing environment and formed in an environment between the ocean basin and the continental margin. From Si–O isotope geochemistry, the original Si source of the study area is thought to relate to a volcanic eruption, which leads to the enrichment of Si in the seawater. The determined values of S isotope in the black rock series of the two study areas both show the characteristics related to organic reduction/biogenic.

Keywords Se-rich siliceous rocks · Geochemistry · Si–O–S isotope · Origin · Sedimentary environment

1 Introduction

Selenium is not only a key nonmetal but also a dispersed element, which is difficult to form an independent deposit with industrial significance (Liu et al. 2005), however, the black rock series, such as the Niutitang Formation at the bottom of Early Cambrian in South China, is important selenium-enriched geological body (Jiang et al. 2007). The Yutangba Selenium Deposit is the first black rock series independent selenium deposit discovered in China and even in the world. The early exploration confirmed about 50 tons of metal selenium reserves (Song and Ding 1989; Yu 1993). The general survey shows that the selenium resources in the Yutangba area can reach 0.01% with the cut-off grade of 0.01% (Feng et al. 2002, 2004, 2009; Liu et al. 2014). Se is also a key nutrient element. Further investigation shows that the distribution area of selenium-rich strata in the Enshi area is 850 km² (Niu et al. 2000; Feng et al. 2004; Zheng et al. 2006), it provides an important guarantee for the development of selenium-rich ecological agriculture in Western Hubei Province.

✉ Caixia Feng
fengcaixia@nwu.edu.cn

¹ State Key Laboratory of Continental Dynamics and Department of Geology, Northwest University, Xi'an 710069, China

² Solid Earth Studies Laboratory, Department of Geology, University of Regina, Regina, SK S4S 0A2, Canada

Therefore, it is becoming a non-traditional mode of mineral resource utilization to search for high selenium strata and develop selenium-rich ecological agriculture.

The Yutangba independent Selenium Deposit is mainly hosted in the Middle-Upper Permian carbonaceous thin-layer siliceous rock shale sequence. In the early exploration process, this set of strata was divided into the third member of the Maokou Formation (Yao 2002; Yao et al. 2002; Feng et al. 2002, 2004, 2009). According to the latest regional stratigraphic progress, the formation is divided into Gufeng formation (Niu et al. 2000; Shi et al. 2016). The Gufeng formation, mainly composed of siliceous rocks and carbonaceous shale, is widely distributed in South China, recording the sedimentary events of the Late Paleozoic East Tethys siliceous rocks (Song and Ding 1989; Yu 1993; Yao 2002; Feng et al. 2002, 2004, 2009). The high selenium anomalies in Gufeng formation are mainly reported in Enshi inter-platform basin (Yao 2002; Feng et al. 2004), which is represented by Yutangba independent Selenium Deposit. The mineralization mechanism of the Yutangba independent Selenium Deposit is still controversial (Yao 2002; Feng et al. 2002, 2009). These studies are mainly focused on the Yutangba deposit itself, but there is still a lack of correlation studies on Se rich strata in large space in the Enshi inter-platform basin.

This study focuses on the Yutangba independent Selenium Deposit and Shadi with high selenium content in the north section. Through element geochemistry and Si–O–S isotope study, the spatial differences of Si–Se in different provenances are revealed. The metallogenic process and metallogenic environment evolution of high Se black rock series are analyzed. Based on summarizing previous research data, the diagenetic and metallogenic model of high selenium black rock series in the Enshi basin is improved, it provides guidance for searching similar Se rich strata.

2 Geological background and deposit geology

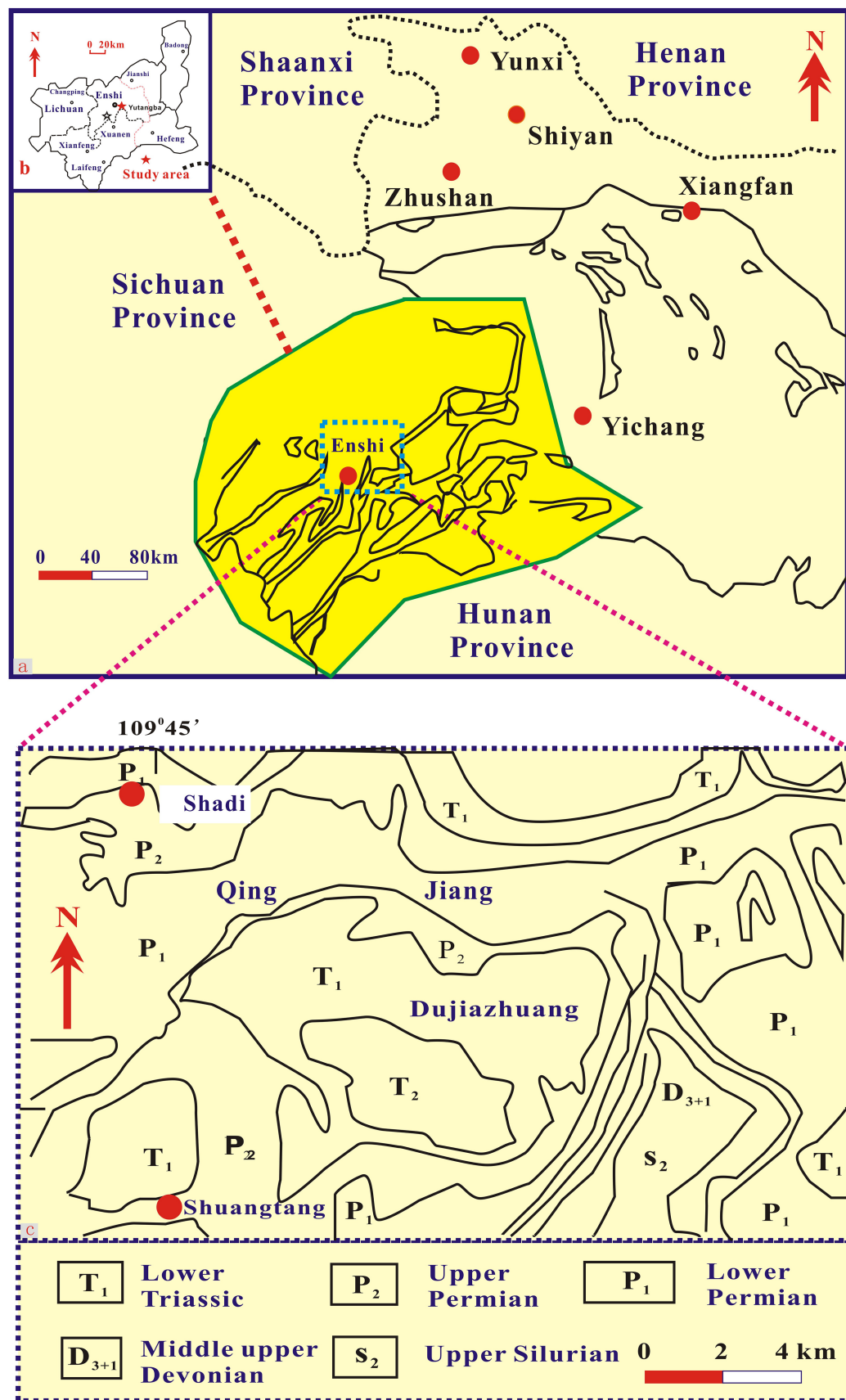
The Enshi Tujia and Miao Autonomous Prefecture, located in the southwest of Hubei Province, occurs at the juncture of the central and western regions of China. It spans $108^{\circ} 23' 12''$ – $110^{\circ} 38' 08''$ E, $29^{\circ} 07' 10''$ – $31^{\circ} 24' 13''$ N. It is connected with Yichang of Hubei Province in the east, Hunan Province in the south, Qianjiang river of Chongqing in the west, Wanzhou of Chongqing in the north and Shennongjia forest region in the northeast (Fig. 1a). The geotectonic position belongs to the middle part of the Yangtze platform and the East Sichuan platform fold belt in the northwest, the Bamianshan platform fold belt of the Upper Yangtze Platform in the southeast, and the Shennongjia fault dome of a fold and fault area occurring in the

Fig. 1 Location **a** Sample points **b** and geological sketch map **c** of the study area (revised from Tian et al 2007)

middle of Hubei Province to the north. Se-rich black rock strata (e.g., the Cambrian Niutitang Formation, the Ordovician–Silurian Longmaxi Formation, the Permian Maokou Formation, and the Triassic Wujiaping, Dalong, and Daye formations) are widely distributed across the Enshi Prefecture (such as Enshi City, Jianshi County, Xuan'en County, Xianfeng County, and Badong County, etc.) (Fig. 1b). The Permian strata are important ore-bearing horizons in southwest Hubei and also to a lesser degree for the whole Province, containing coal, bauxite, pyrite, manganese, vanadium, Se, and other minerals (Zhou and Huang 2010). The Se resources in the Enshi Prefecture are distributed across Bajiao-Shengjia, Mufu-Banqiao, Xiangjiacun-Qiyangba, Luozhentian-Mazhe-Tiechangshuo, Shuanghe-Hongtuxi-Shiyao, Zhongjianhe-Huangcun-Shadi, and other places. The Se reserves are very large and hosted at shallow depths. The exposed area of Se-bearing carbonaceous shale and coal is about 850 km^2 , divided into two zones: one in the north and another, the south. The thickness of the ore-bearing strata is between 3.6 and 9.0 m (Guo 2012).

The outcropping strata in the study area are mainly Permian and Triassic strata, which include the Lower Permian Maokou Formation (P_{1m})-this formation is divided into upper and lower two Sects. (1) lower section (P_{1m1+2}): chert nodule-bearing bioclastic limestone, bioclastic argillaceous limestone; (2) upper section (P_{1m3}): limestone, a sequence of carbonaceous siliceous rock, carbonaceous shale with siliceous rock, dolomite and carbonaceous siliceous rock occur on top of the lens body (Regional geology of Hubei Province 1990; this formation is termed the Gufeng Formation in the literature (Niu et al. 2000). The Upper Permian Wujiaping Formation (P_{2w}) contains coal and siliceous rocks, while the Upper Permian Dalong Formation (P_{2d}) contains siliceous rocks and dolomites. The Triassic Daye Formation comprises limestone (T_{1d}) (Fig. 2; Song and Ding 1989; Regional geology of Hubei Province 1990).

The upper section of the Lower Permian Maokou Formation (P_{1m3} /Gufeng Fm.) is the main Se bearing layer, chiefly comprising a 13 m thick set of black, shallow marine laminated carbonaceous silicalite, which is divided into three sequences. From top to bottom these are (1) light gray and black shale and mudstone layers, 3.0 m in thickness, with a Se content generally in the range, 4.0–180 $\mu\text{g/g}$; (2) black thinly-layered carbonaceous siliceous rock occurring with black siliceous carbonaceous shale, with a total thickness of 6.55 m, and Se content of



Mesozoic		Triassic		Lower Triassic		Jialing River Group			
Palaeozoic		Permian		Upper Permian		Wujiaping formation	Dalong formation		

Fig. 2 Photos of variously occurring, lithology and stratigraphic column of the siliceous rocks in Enshi, Hubei Province (Hubei Provincial Bureau of Geology and Mineral Resources, 1990) **a** Thick layer siliceous rock in Shadi County; **b** Thick layer siliceous rock with thin black shale in Shadi County; **c** -Medium-thick siliceous rock with thin layer black shale in Yutangba, Shuangtang country; **d** -thin layer siliceous rock with thin layer black shale

100–2590 µg/g, to a maximum of 8390 µg/g; (3) black thinly-layered carbonaceous siliceous rock with black carbonaceous shale, with a thickness of 3.54 m, and a Se content mainly in the range, 47–350 µg/g, but locally can reach, 1120–5400 µg/g (Fig. 2; Feng et al. 2004).

Yutangba independent Se Deposit in Enshi is located at Xiaba village, Xintang, 82 km southeast of Enshi City (Fig. 1c). It is regionally located in the middle part of the northeast section of the fold belt of the Yangtze platform and the middle part of the northwest wing of Shuanghe syncline (Song and Ding 1989). The exposed rock in the dam is mainly Triassic limestone, and the Se-rich ore belt is the siliceous rocks of the Permian Maokou Formation, which is distributed in roughly an east–west direction. The main form of the Se ore body is a stratified lens, which has no obvious boundary with the surrounding rock. Its length is generally tens of m to more than 100 m, and the average thickness is between 0.7 and 5.0 m. The geological occurrence is consistent with that of stratified rock, with a regional NE-SW strike of 160° and a dip angle of about 60°. The average Se content (%) is between 0.032 and 0.451 (Song and Ding 1989; Yu 1993; Feng et al. 2004). The main components of the ore are quartz (51.7%), chalcedony (11.9%), carbonaceous material (17.8%), and hydromica (11.6%). Minor minerals include pyrite, hematite, limonite, dolomite, fluorite, vanadyl, biotite, epidote, rutile, and selenite (Yu 1993).

Shadi township is located to the northeast of Enshi City, in Hubei Province (Fig. 1c), situated on the North Bank of the middle reaches of the Qingjiang River. Shadi Township essentially represents a slope, surrounded by water on three sides and a mountain on the other side. The main rock types are limestone, carbonaceous slate, carbonaceous shale, and carbonaceous siliceous rock (Yu et al. 2018).

3 Sample collection and test methods

3.1 Sample collection and lithology description

The samples studied were collected from the No.5 ore body of the Yutangba selenium mining area in Xiaba village, Shuangtang Township, Enshi City, and the high selenium mineralization point in Huabei village, Shadi Township (Fig. 1c). The profile rocks are well developed. Sampling

of the high Se stratum was systematic and densely spaced, with fresh samples collected wherever possible by trenching of the strata. In this study, more than 40 rock samples (from bottom to top of study strata, Fig. 2a–d) were collected for testing and analysis. Guided by the results of previous investigations in these areas, our work included detailing the thickness and lithological characteristics of the siliceous rocks and coal-bearing strata which are rich in Se.

The nature of field rock characters of two study areas is markedly different (Fig. 2a–d). Figs. 2a and b illustrate the near-horizontal layering of Se-rich black rock strata from Shadi. The lithologies of this section, from bottom to top are siliceous rock, siliceous shale, carbonaceous shale, and calcareous mudstone. Gypsum was observed in some layers on the surfaces of the rock strata. Figs. 2c and d are of strata exposed at the No. 5 Se-ore body, Yutangba Se deposit, with strata trending at 155°–172° and with a dip angle of 52°–65° and occurs phase transition from a thick layer siliceous rocks and shale to thin layer siliceous rocks and shale. The lithologies of this section from bottom to top are a thick layer of grey limestone containing chert nodules that are overlain by a thin black layer of carbon silicalite and carbonaceous shale, a 2.0–3.0 mm thick layer of sapropel, and a moderately thick layer of interblended light grey to black shale and yellow mudstone with light gray shale.

3.2 Major and trace element determinations

The collected samples were cleaned with distilled water and dried in an oven at 65 °C. After which these were crushed with an agate pestle and mortar and passed through a 200 mesh nylon screen, before the determination and analysis of major and trace element compositions. The analysis was completed in the State Key Laboratory of Ore Deposit Geochemistry, Institute of Geochemistry, Chinese Academy of Sciences, Guiyang, China. The major element analysis was completed by X-ray fluorescence spectrometry (utilizing a Philips PW4400 XRF instrument). The data quality of replicate samples and the standard reference materials, GSR-1 and GSR-3, were monitored during the analysis process. The analytical accuracy was determined to be better than 3 %.

The analysis of trace elements was completed using an ELAN6000 Inductively Coupled Plasma-Mass Spectrometer system, with data quality, monitored by analysis of standard reference materials, OU-6, and GBPG-1. The determined analytical accuracy was better than 5 % (Qi et al. 2000).

Se content was tested by $\text{HNO}_3 + \text{HF} + \text{HClO}$ digestion method, and determined by hydride generation atomic fluorescence spectrometry (AFS-920). Standard reference

materials GBW07105 and GBW07107 were used for quality control, and the analysis error was less than 10 %. Detailed technical process can be seen in Fan et al. (2005).

3.3 Silicon (Si) and oxygen (O) isotope

The analysis of Si and O isotopes was completed at the Key Laboratory of Isotope Geology, Ministry of Land and Resources, Beijing, China.

First, the sample was crushed down to less than 200 mesh size. It was then soaked in dilute hydrochloric acid, washed repeatedly with distilled water, and then dried in air. For the determination of silicon isotopes (for the samples contained impurities, such as S and C) the samples required advance chemical treatment, pure Na₂CO₃ added to the sample within a platinum crucible that was then melted at 1000 °C, thereafter to be dissolved with 7.4 N HCl, which allowed amorphous hydrated SiO₂ to precipitate out of the solution. The samples were then rinsed, repeatedly with 3.0 N HCl, 1.5 N HCl, and high-purity water, after which these were ignited at 1200 °C for 30 min. In addition to SiF₄, there were also small amounts of Si₂F₆ in the reaction product, which could be removed by a cold trap to improve analytical accuracy. Silica can further be purified by oxidation, where after the SiO₂ was purified by the interaction with BrF₅ to form SiF₄, which was then analyzed on the Finnigan MAT-251EM mass spectrometer. NBS-28, a quartz sand sample standard of the National Bureau of Standards, was selected as the standard sample, and the analytical accuracy for this method was determined as 0.1 ‰.

The method of BrF₅ (Clayton and Mayeda 1963) was used for the determination of oxygen isotopes, whereby oxygen is extracted from the siliceous rock powder and converted into CO₂, which was then analyzed on the Finnigan MAT-251 EM mass spectrometer. The analytical accuracy was better than 0.2 ‰. The results of the oxygen isotopic work being expressed in $\delta^{18}\text{O}$ Vienna-Standard mean ocean water (V-SMOW).

3.4 Sulfur (S) isotope

S isotope analysis of pyrite was determined after heating of the samples and cuprous oxide in a vacuum, which resulted in an oxidation reaction to generate SO₂ gas. After purification, the sulfur isotope composition was analyzed on a Finnigan MAT251 gas isotope mass spectrometer. The experimental work was carried out in the State Key Laboratory of Environmental Geochemistry, Institute of Geochemistry, Chinese Academy of Sciences, Guiyang, China. The results are expressed in $\delta^{34}\text{S}$ notation and the relative standard is the Vienna-Canyon Diablo Troilite (V-CDT).

4 Results

4.1 Major elements

The analysis results for major elements of various rocks studied in the black rock series in Table 1. The lithology of the black rock series in Shadi County is relatively simple. The content of SiO₂ in siliceous rocks and carbonaceous siliceous rocks ranges from 69.75 wt% to 93.24 wt% and the content of other oxides is relatively low. The SiO₂ content of the carbonaceous siliceous shale ranges from 55.10 wt% to 55.76 wt%. The overall variation range is not large. The Al₂O₃ content is higher than for other lithologies (up to 9.40 wt%), and the loss on ignition loss of ignition (LOI) is also higher (between 27.85 wt% and 30.65 wt%). The SiO₂ content of carbonaceous shale ranges from 21.92 wt% to 31.78 wt%, and the LOI is from 42.58 wt% to 45.12 wt% (Table 1). By contrast, the lithologies of the Yutangba mining area is relatively complex, and the samples include carbonaceous siliceous shale, carbonaceous siliceous rock, sapropel, siliceous rock, and siliceous shale with oxidized pyrite layers (Table 1). The SiO₂ content of carbonaceous siliceous shale ranges from 51.91 wt% to 68.85 wt%, with a wide range of variation, and the content of other oxides are relatively low. The SiO₂ content of two siliceous shales with oxidized pyrite layers ranges from 58.42 wt% to 76.89 wt%. One reason why the content range changes greatly are that the carbon content of one sample is high and its LOI value is as high as 32.02 wt%. The Al₂O₃ content of two sapropel coal samples is higher than that of the other samples (from 10.65 wt% to 19.02 wt%). The SiO₂ content of siliceous rock samples is more than 90.42 wt%, while the other oxides are relatively low. The CaO content of Triassic limestone s is 51.73 wt%, and its LOI is 37.05 wt%.

4.2 Trace elements

Relative to the abundance of elements in the crust, the investigated samples of carbonaceous siliceous shale, calcareous shale, sapropel coal seam, limestone, and siliceous rock in the Yutangba area are characterized by enrichment in ferrophilic elements (Mo, Co, and Ni), parent Cu elements (Cu, As, Sb and Pb), rich lithophile elements (V and Cr), and depletion in Rb, Sr, Ba, U, Th, Bi, and Zn (Table 2). By contrast, the carbonaceous siliceous shale, calcareous shale, and siliceous rock in the Shadi horizons are rich in ferrophilic elements (e.g., Mo, Co, and Ni), parent Cu elements (As, Sb, Zn, and Pb), and also rich in lithophile elements (V, Cr, Sr, and U), and Rb, Ba, and Th. However, they are depleted in Cu and Bi (Table 2).

Table 1 Major element contents (wt.%) of black rock series in Enshi, Hubei Province, China

Sample nos	Lithology	SiO ₂	Al ₂ O ₃	Fe ₂ O ₃	MgO	CaO	Na ₂ O	K ₂ O	MnO	P ₂ O ₅	TiO ₂	LOI	Total	Al/(Al + Fe + Mn)	MnO/TiO ₂
YTB-3	Carbonaceous siliceous shale	49.82	6.63	1.36	1.10	0.48	0.20	1.74	0.03	0.07	0.18	38.20	99.80	0.58	0.15
YTB-2	Carbonaceous siliceous shale	51.91	4.72	2.32	0.81	0.56	0.09	1.44	0.03	0.06	0.17	37.30	99.41	0.36	0.18
YTB-a	Carbonaceous siliceous shale	62.25	6.50	5.58	0.59	0.45	0.06	1.84	0.05	0.06	0.20	22.32	99.89	0.25	0.23
YTB10-3-1	Sapropelite	47.86	19.02	2.85	0.46	0.54	0.11	0.90	0.01	0.12	0.31	27.95	100.13	0.65	0.03
YTBZ-10-1-a	Siliceous rock	85.86	3.75	4.19	0.22	0.69	1.06	0.27	0.09	0.05	0.10	3.75	100.02	0.20	0.87
YTBZ-13-1	Sapropelite	33.96	15.13	1.72	0.88	1.09	0.85	2.12	0.05	0.05	0.26	43.94	100.06	0.71	0.20
YTBZ-6	Carbonaceous siliceous shale	66.47	5.40	1.86	0.57	0.46	0.10	0.45	0.02	0.05	0.13	24.35	99.86	0.45	0.16
YTB10-4-1	Carbonaceous siliceous rock	67.32	11.00	2.45	1.62	0.30	0.21	2.54	0.03	0.06	0.20	14.38	100.12	0.56	0.17
YTBZ-26	Carbonaceous siliceous rock	59.84	0.52	0.62	1.42	0.57	0.14	1.65	0.02	0.05	0.06	35.30	100.18	0.19	0.28
YTB10-1	Carbonaceous siliceous rock	67.00	10.65	1.52	0.24	0.30	0.08	0.43	0.01	0.06	0.15	19.63	100.07	0.66	0.08
YTB-6	Carbonaceous siliceous rock	92.83	0.30	0.24	0.15	0.12	0.01	0.05	0.05	0.05	0.07	5.55	99.42	0.23	0.76
YTB-8	Carbonaceous shale	57.17	5.11	1.56	1.19	0.57	0.12	1.53	0.02	0.07	0.12	32.38	99.84	0.48	0.13
YTB10-2	Carbonaceous siliceous shale	68.63	8.35	1.39	0.61	0.32	0.15	1.96	0.01	0.05	0.15	18.47	100.09	0.63	0.07
YTB10-18	Siliceous shale	58.42	5.33	1.52	0.56	0.58	0.10	1.12	0.01	0.06	0.14	32.02	99.86	0.50	0.09
YTB10-1a-1	Siliceous rock	82.50	2.26	0.67	0.38	0.32	0.07	0.41	0.02	0.06	0.12	13.31	100.12	0.49	0.06
YTB-1	Carbonaceous siliceous shale	62.70	1.40	1.61	0.73	1.24	0.08	1.37	0.01	0.06	0.10	30.84	100.14	0.20	0.10
YTB-4	Carbonaceous siliceous shale	79.03	2.18	0.85	0.29	0.57	0.14	0.45	0.02	0.06	0.13	16.07	99.79	0.42	0.12
YTB-5	Siliceous rock	91.20	1.34	0.48	0.45	0.22	0.06	0.31	0.01	0.06	0.10	5.59	99.82	0.44	0.11
YTBZ-12a	Siliceous rock	90.42	1.29	0.53	0.11	0.94	0.07	0.08	0.01	0.05	0.10	6.25	99.85	0.41	0.08
YTB10-17	Siliceous rock	76.89	4.37	0.74	1.07	0.26	0.09	0.97	0.01	0.07	0.16	15.22	99.85	0.62	0.08
YTB10-7-1	Siliceous rock	68.85	2.28	1.52	0.78	0.45	0.10	1.45	0.01	0.05	0.12	24.47	100.08	0.30	0.08
SD10-1	Siliceous rock	69.75	0.76	0.92	3.12	5.18	0.15	0.46	0.01	0.05	0.10	19.32	99.82	0.19	0.12
SD10-2	Siliceous rock	64.56	0.57	1.15	4.47	6.84	0.24	0.88	0.01	0.05	0.09	21.17	100.02	0.12	0.12
SD10-3	Siliceous rock	92.15	0.27	0.36	0.16	0.34	0.12	0.30	0.01	0.04	0.07	6.05	99.87	0.17	0.10
SD10-7	Calcareous shale	27.92	0.52	0.41	8.83	17.12	0.46	2.12	0.02	0.05	0.10	42.58	100.13	0.26	0.15
SD10-8	Siliceous rock	93.24	0.31	0.39	0.24	0.21	0.11	0.44	0.01	0.04	0.07	4.65	99.71	0.18	0.14
SD10-9	Siliceous rock	92.30	0.35	0.32	0.14	0.23	0.10	0.29	0.01	0.04	0.07	5.95	99.80	0.23	0.12
SD10-12	Siliceous rock	79.32	2.00	0.45	1.63	2.71	0.14	0.43	0.05	0.10	0.17	13.10	100.10	0.53	0.31
SD10-19	Carbonaceous shale	55.76	9.40	0.63	1.40	0.50	1.03	2.87	0.01	0.15	0.22	27.85	99.82	0.81	0.05
SD10-22	Carbonaceous shale	55.10	8.02	0.68	1.25	0.42	1.00	2.64	0.01	0.12	0.20	30.65	100.09	0.77	0.05
SD10-14-1	Calcareous shale	31.22	5.20	0.56	1.45	13.26	0.77	2.19	0.01	0.10	0.15	45.12	100.03	0.72	0.05
SD10-14-2	Siliceous rock	88.15	1.76	0.27	0.59	1.49	0.10	0.31	0.01	0.06	0.15	7.04	99.93	0.65	0.03
SD10-14-1a	Calcareous shale	31.78	6.04	1.15	1.42	12.29	0.78	2.16	0.01	0.05	0.10	44.02	99.80	0.60	0.10

Table 2 Trace element contents (ppm) and relative parameters of black rock series in Enshi, Hubei Province, China

Sample nos	Lithology	V	Cr	Co	Ni	Cu	Zn	As	Mo	Rb	Sr	Ba	Pb	Bi	Th	U	Se	U/Th	δU	V/(V + Ni)	
YTB-3	Carbonaceous siliceous shale	3550	1120	69.8	427	38.1	29.6	5.25	354	42.4	54.5	18.3	96.5	32.4	0.53	8.44	33.8	577	4.00	1.85	0.89
YTB-2	Carbonaceous siliceous shale	1910	549	18.2	266	17.6	18.9	6.77	562	34.0	19.4	20.3	11.5	36.0	0.45	3.78	34.3	1639	9.07	1.93	0.88
YTB-a	Carbonaceous siliceous shale	1430	302	66	260	124	173	24.6	109	54.7	35.9	10.4	141	35.2	0.50	9.31	10.5	107	1.13	1.54	0.85
YTB10-3-1	Sapropelite	1950	1570	51.6	101	143	48.3	37.1	170	15.8	36.5	37.8	75.7	36.8	0.40	1.78	124	28.1	69.7	1.99	0.95
YTB10-4-1	Carbonaceous siliceous rock	4630	859	95.4	125	34.1	53.9	17.7	447	60.8	6.05	22.0	93.2	21.6	1.19	6.49	13.1	680	2.02	1.72	0.97
YTBZ-26	Carbonaceous siliceous rock	3750	1820	57	416	27	22.1	5.49	1314	43.2	18.7	9.20	80.6	19.6	0.62	8.79	46.6	1788	5.30	1.88	0.90
YTB-6	Carbonaceous siliceous rock	799	201	230	33.5	45.1	19	5.16	124	3.70	16.3	14.1	20.2	18.5	0.26	0.33	9.73	39.2	29.9	1.98	0.96
YTB10-2	Carbonaceous siliceous shale	883	473	50.3	104	34.7	43.8	12.4	109	57.6	23.7	23.0	171	30.2	0.50	5.86	9.46	1346	1.61	1.66	0.89
YTB10-18	Siliceous shale	3960	1210	173	361	102	24	7.97	395	28.1	21.7	15.3	62.8	29.9	0.44	2.40	51.2	408	21.3	1.97	0.92
YTB-1	Carbonaceous siliceous shale	1990	925	62.8	228	49.4	23.6	6.91	417	32.2	116	7.26	92.7	31.3	0.34	3.51	52.4	28.5	14.9	1.96	0.90
YTB	Carbonaceous siliceous shale	800	810	29.1	62.17	44.1	19.1	21.4	125	25.7	19.6	5.73	82.6	19.4	0.26	2.87	30.1	107	10.5	1.94	0.93
A		16.3	7.04	3.32	2.67	1.07	0.57	6.75	262	0.34	0.09	32.9	0.20	2.02	0.26	0.64	1.82	7667			
SD10-1	Siliceous rock	1910	308	55.6	164	16.83	180	17.5	24.3	8.05	290	3.83	29.6	3.05	0.06	0.62	6.83	51.2	11.1	1.94	0.92
SD10-2	Siliceous rock	1860	234	33.1	166	27.07	221	20.0	186	21.0	549	4.95	67.8	8.17	0.12	1.90	16.8	57.1	8.85	1.93	0.92
SD10-3	Siliceous rock	1536	235	32.6	167	26.80	224	19.8	186	20.7	545	4.93	67.4	8.28	0.13	1.97	17.0	59.9	8.61	1.93	0.90
SD10-3-1	Siliceous rock	1667	86.3	169	172	29.92	269	18.1	99.0	5.49	148	2.27	35.6	10.4	0.05	0.60	7.31	58.1	12.2	1.95	0.91
SD10-7	Calcareous shale	3960	828	52.6	668	89.05	792	21.0	421	38.5	795	10.0	110	26.2	0.42	3.14	39.9	120	12.7	1.95	0.86
SD10-8	Siliceous rock	688	241	159	28.4	6.34	20.5	12.6	23.5	12.1	20.7	2.15	42.0	9.81	0.13	0.53	4.57	47.6	8.58	1.93	0.96
SD10-9	Siliceous rock	799	130	116	67.6	13.0	34.5	18.7	52.5	5.72	35.1	1.21	36.2	9.81	0.06	0.41	6.10	38.2	15.0	1.96	0.92
SD10-12	Siliceous rock	882	412	95.6	115	21.8	197	17.4	31.8	10.1	308	3.00	48.4	10.3	0.06	0.84	6.69	71.4	7.93	1.92	0.88
SD10-19	Carbonaceous siliceous shale	600	806	21.2	23.9	67.9	18.7	16.9	24.1	87.2	51.6	6.99	281	49.01	2.97	16.6	26.4	31.7	1.59	1.65	0.96
SD10-14-1	Calcareous shale	1019	979	24.14	685	130	1001	26.7	747	45.1	735	14.0	112	28.3	0.63	4.67	60.1	118	12.9	1.95	0.60
B		10.7	3.73	3.02	3.28	0.93	4.61	9.92	166	0.26	1.01	12.6	0.19	1.28	0.25	0.44	1.08	965			
C		143	127	24.7	81.3	56	76.3	2.03	1.43	108	382	0.51	463	14	1.90	7.60	20.7	0.08			

The analysis results of dispersed element Se in various samples of black rock series in the study area are listed in Table 2. It can be seen that all kinds of samples have obvious Se enrichment characteristics compared with Se abundance in the crust, and the enrichment of samples in the Yutangba Se independent deposit is greater than that in the Shadi Se enrichment area.

In the crustal abundance normalized diagram (Fig. 3), the rock samples from the two study areas are enriched with respect to Se, Mo, Sb and Pb.

4.3 Rare earth elements (REE)

REE analysis results and relevant parameter of various samples of the black rock series as studied are listed in Table 3.

In the Yutangba area, the total amount of REE in different types of black rock series strata (carbonaceous siliceous rock, siliceous rock, carbonaceous siliceous shale, calcareous shale and limestone) varies greatly (8.63–106 ppm), with an average of 68.3 ppm. The LREE/HREE ratio of a sample can reflect its degree of REE differentiation. The larger the ratio, the more enriched in

LREE the sample is. The LREE/HREE ratio in the study area is 2.19–7.52, with an average of 5.16. The average value of La_N/Yb_N is 6.60, with light rare earth being relatively enriched. δCe_N is from 0.39 to 0.95, with an average value of 0.59, and Ce that displays a slightly weak negative anomaly. δEu_N is from 0.49 to 0.83, with an average value of 0.68, which displays a slight Eu negative anomaly. On the chondrite-normalized REE diagram (Fig. 4a), the samples of Yutangba in Shuangtangxiang all incline to the right. Furthermore, on the shale in North America normalized plot, the REE curves of the black rock series from Yutangba in Shuangtangxiang are nearly all parallel, which indicates that the source areas are relatively consistent (Fig. 4b).

The total amount of REE in different types of black rock series (carbonaceous siliceous rock and carbonaceous siliceous shale) in the Shadi area changes greatly (4.05–167 ppm), with an average value of 51.1 ppm; the LREE/HREE ratio is 3.34–10.35, with an average value of 4.93; the La_N/Yb_N average value is 5.89, and light rare earth is relatively rich; $\delta\text{Ce}_N = 0.43\text{--}1.05$, with an average value of 0.56, and Ce trends from weak negative anomaly to weak positive anomaly; $\delta\text{Eu}_N = 0.11\text{--}0.17$, the average value is 0.13, with an Eu negative anomaly. On the chondrite-normalized REE diagram (Fig. 4c), the REE model curves of samples in Shadi all tilt to the right. Whereas on the shale in North America normalized plot (Fig. 4d), the REE curve of the samples in Shadi has no obvious tilt to the left or right, and the distribution is nearly horizontal as a whole.

4.4 Si, O and S isotopes

In the Yutangba selenium mining area, the $\delta^{30}\text{Si}_{\text{NBS}-28}$ value for siliceous rock is in the range of 0.6–1.6‰, and the $\delta^{18}\text{O}_{\text{V-SMOW}}$ value of siliceous rock is in the range of 25.0–27.3‰ (Table 4). The values of $\delta^{30}\text{Si}_{\text{NBS}-28}$ and $\delta^{18}\text{O}_{\text{V-SMOW}}$ of siliceous rocks in the Se enriched area of black rock series in Shadi are in the range of 0.9–1.3‰ and 25.7–26.3‰. In addition, the values of $\delta^{34}\text{S}_{\text{V-CDT}}$ of pyrite single mineral samples selected from the two study areas range from –49.27‰ to –19.23‰ and from –23.45‰ to –21.66‰ (Table 5). From Table 5, it can be seen that the S isotope in Yutangba mining area varies greatly, while that in Shadi has a relatively small isotopic variability.

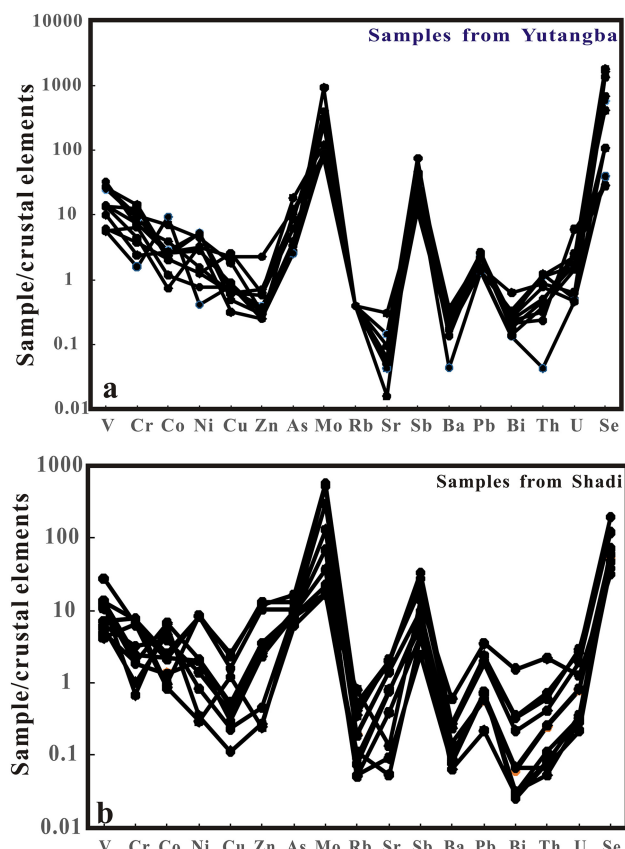


Fig. 3 Trace elements spider diagram of the Se-rich siliceous rocks in Enshi, Hubei Province (Abundance values of crustal elements according to Li Tong 1992)

Table 3 REE contents (ppm) and relative parameters of black rock series in Enshi, Hubei Province, China

Sample nos	Lithology	La	Ce	Pr	Nd	Sm	Eu	Gd	Tb	Dy	Ho	Er	Tm	Yb	Lu	Σ REE	LRREE/HREE	$\text{La}_{\text{N}}/\text{Yb}_{\text{N}}$	$\delta\text{Eu}_{\text{CN}}$	$\delta\text{Ce}_{\text{CN}}$	$\delta\text{Eu}_{\text{SN}}$	$\delta\text{Ce}_{\text{SN}}$	(La/Ce) SN
YTB-3	Carbonaceous siliceous shale	25.0	30.8	5.21	18.9	3.51	0.78	3.11	0.50	2.86	0.67	1.86	0.27	1.66	0.27	95.39	7.52	10.80	0.70	0.63	1.07	0.63	1.74
YTB-2	Carbonaceous siliceous shale	20.5	25.9	3.81	13.7	2.19	0.36	2.27	0.37	2.55	0.60	1.71	0.25	1.60	0.23	75.84	7.09	9.19	0.49	0.67	0.74	0.68	1.70
YTB-a	Carbonaceous siliceous shale	16.3	32.5	4.04	15.1	3.05	0.64	3.01	0.50	3.07	0.70	2.07	0.31	2.17	0.36	83.83	5.87	5.39	0.63	0.95	0.96	0.94	1.08
YTB10-3-1	Sapropelite	16.2	15.2	3.26	12.4	2.69	0.63	2.75	0.44	2.71	0.63	1.91	0.29	2.10	0.32	61.52	4.52	5.53	0.70	0.48	1.06	0.49	2.29
Ytb10-4-1	Carbonaceous siliceous rock	5.84	8.93	2.22	12.1	4.61	1.28	4.78	0.83	4.69	0.96	2.46	0.30	1.73	0.22	50.94	2.19	2.42	0.83	0.61	1.24	0.57	1.40
YTBZ-26	Carbonaceous siliceous shale	24.0	25.0	5.61	23.6	5.37	1.29	5.68	0.96	5.63	1.29	3.61	0.47	3.28	0.47	106.25	3.97	5.25	0.71	0.51	1.06	0.51	2.06
YTB-6	Carbonaceous siliceous rock	2.47	1.98	0.48	1.77	0.40	0.08	0.41	0.06	0.36	0.11	0.24	0.04	0.21	0.04	8.63	4.92	8.32	0.59	0.42	0.90	0.43	2.68
YTB10-2	Carbonaceous siliceous shale	15.5	26.1	3.53	12.4	1.94	0.42	1.94	0.32	1.84	0.46	1.34	0.20	1.48	0.23	67.69	7.67	7.51	0.65	0.83	0.99	0.83	1.27
YTB10-18	Siliceous shale	13.0	10.0	2.78	12.2	2.50	0.70	2.61	0.47	2.81	0.66	1.79	0.27	1.75	0.26	51.79	3.88	5.33	0.83	0.39	1.24	0.39	2.79
YTB-1	Carbonaceous siliceous shale	23.0	19.6	4.38	17.6	3.71	1.08	4.45	0.73	4.67	1.12	3.11	0.43	2.75	0.43	87.06	3.92	6.00	0.81	0.45	1.2	0.45	2.52
YTB	Carbonaceous siliceous shale	16.6	17.1	3.07	12.8	2.42	0.43	2.52	0.40	2.62	0.57	1.74	0.25	1.74	0.27	62.52	5.18	6.83	0.53	0.55	0.79	0.56	2.07
SD10-1	Siliceous rock	3.70	3.00	0.68	2.87	0.55	0.14	0.65	0.11	0.80	0.18	0.61	0.10	0.71	0.12	14.21	3.34	3.73	0.70	0.43	1.04	0.44	2.65
SD10-2	Siliceous rock	8.87	8.96	1.45	5.82	1.12	0.24	1.20	0.18	1.33	0.31	0.90	0.14	0.94	0.15	31.61	5.13	6.77	0.62	0.56	0.93	0.57	2.12
SD10-3-1	Siliceous rock	8.80	8.84	1.41	5.69	1.07	0.27	1.17	0.18	1.23	0.28	0.90	0.13	0.95	0.15	31.08	5.23	6.66	0.73	0.56	1.1	0.57	2.14
SD10-3	Siliceous rock	2.26	2.49	0.46	1.93	0.45	0.11	0.58	0.09	0.58	0.12	0.37	0.05	0.37	0.05	9.91	3.48	4.38	0.64	0.57	0.94	0.57	1.95
SD10-7	Calcareous shale	23.0	20.9	4.15	17.2	3.47	0.74	3.76	0.58	3.71	0.89	2.64	0.36	2.50	0.41	84.39	4.68	6.61	0.62	0.49	0.93	0.5	2.36
SD10-8	Siliceous rock	1.30	1.20	0.14	0.45	0.07	0.02	0.09	0.02	0.16	0.05	0.18	0.03	0.29	0.05	4.05	3.67	3.26	0.87	0.57	1.29	0.61	2.32
SD10-9	Siliceous rock	1.70	1.91	0.31	1.16	0.23	0.04	0.25	0.04	0.25	0.06	0.18	0.03	0.17	0.03	6.35	5.32	7.28	0.55	0.60	0.83	0.61	1.90
SD10-12	Siliceous rock	4.71	3.88	0.85	3.29	0.64	0.13	0.76	0.13	0.81	0.20	0.67	0.10	0.70	0.12	16.99	3.87	4.82	0.55	0.44	0.82	0.45	2.60
SD10-19	Carbonaceous siliceous shale	36.8	76.1	7.77	26.7	4.35	0.76	3.37	0.49	3.10	0.78	2.74	0.43	3.28	0.54	167.13	10.35	8.04	0.59	1.05	0.91	1.05	1.04
SD10-14-1	Calcareous shale	28.2	24.5	5.04	20.6	4.16	0.86	4.67	0.69	4.91	1.15	3.47	0.47	3.15	0.50	102.30	4.38	6.43	0.60	0.46	0.89	0.47	2.48
SD10-14-19	Calcareous shale	26.5	23.3	4.64	19.2	3.76	0.80	3.89	0.64	4.25	0.97	2.92	0.42	2.78	0.46	94.43	4.78	6.84	0.63	0.47	0.95	0.48	2.44

5 Discussion

5.1 Redox conditions and sedimentary environment

5.1.1 Evidence from major element compositions

Previous studies have shown that the content of TiO_2 is mainly related to the intervention of terrigenous materials, while MnO is a sign of the deep ocean. The MnO/TiO_2 ratios for black rock series deposited in a continental slope and marginal sea is generally less than 0.5, while this ratio for black rock series deposited in distant ocean basin is more than 0.5 (Sugisaki et al. 1982). The MnO/TiO_2 ratios for the investigated suite of black rock series samples in the Shadi and Yutangba areas range from 0.03 to 0.31 and from 0.03 to 0.78 (Table 1), respectively. These values indicate that the black rock series in the two study areas may have formed near the continental slope and margin sea, and the black rock series in the Yutangba area is farther away from the continental slope than that in the Shadi area.

The Al_2O_3 , Fe_2O_3 and TiO_2 contents of black rock series play an important role in judging their environment of formation (Murray et al. 1990; Murray 1994; Girty et al. 1996). When all the data are plotted using the sedimentary discrimination diagram of $\text{Fe}_2\text{O}_3/\text{TiO}_2\text{-Al}_2\text{O}_3/(\text{Al}_2\text{O}_3 + \text{Fe}_2\text{O}_3)$ (Fig. 5), it can be observe that the black rock series in both study areas fall into the field of a continental margin sedimentary environment (e.g. 0.5–0.9; Murray 1994).

5.1.2 Evidence from trace element contents

As an index to help judge the redox environment of an area, the variation range of δU (i.e., $\delta\text{U} = 6\text{U}/(3\text{U} + \text{Th})$) plays an important role. If the $\delta\text{U} > 1.0$, this indicates an anoxic environment, whereas δU values of < 1.0 indicate it is normal seawater (Wignall 1994). The δU values of the black rock series samples in the two study areas are both greater than 1.0 (1.54–1.98, 1.65–1.95; Table 2), implying that the sedimentary environment of black rock series in this area is one that was reducing.

Similarly, the U/Th ratio can be used as a parameter to help identify the redox environment. Such that, if $\text{U}/\text{Th} > 1.25$, this represents an anoxic environment, whereas values of between $0.75 < \text{U}/\text{Th} < 1.25$ represents a poorly oxygenated environment, and $\text{U}/\text{Th} < 0.75$ represents an oxidizing environment (Jones and Manning 1994). The U/Th ratio of Se-rich black rock series in the Yutangba mining area and the Shadi area falls to 1.13–69.7 and 1.59–15.0, respectively (Table 2). As such these values

also suggest an anoxic sedimentary environment for deposition in both study areas.

In addition, V and Ni belong to the same group of elements to iron. For this reason, their ionic valence changes with the degree of oxidation. They are mainly adsorbed and precipitated by colloidal particles or clay, but V is easily adsorbed and enriched in the oxidation environment, while Ni is more easily enriched in the reduction environment. Therefore, the $\text{V}/(\text{V} + \text{Ni})$ ratio of the elements can reflect the redox environment of the precipitated water body (Arthur and Sageman 1994; Rimmer 2004). When the $\text{V}/(\text{V} + \text{Ni})$ ratio is greater than 0.54, this indicates that the environment of sediment formation is marine, and an anoxic environment; where a $\text{V}/(\text{V} + \text{Ni})$ ratio of less than 0.46 indicates that the sedimentary environment is an oxidizing one (Dill 1986). The $\text{V}/(\text{V} + \text{Ni})$ ratios for the investigated samples from Yutangba mining area are all greater than 0.54, with a maximum value of as high as 0.97, while the Shadi samples are between 0.60 and 0.96. The above data show that the sedimentary environment of selenium rich strata in the black rock series in the Enshi research area is a reducing environment (i.e., one of hypoxia) (Table 2).

5.1.3 Evidence from rare earth element compositions

δCe and δEu can reflect the enrichment and depletion of Ce and Eu, respectively, which may then be used to help determine the source of genetic materials, and of the oxidation-reduction environment of the ancient ocean. The relationship between Ce anomaly and sea level fluctuation indicates that to a greater degree, water depth controls the redox state and that a loss of Ce reflects bottom water. When sea-level rises, the concentration of dissolved oxygen in bottom water decreases, and the abnormal value of Ce in sediment tends to decrease. When sea-level falls, the concentration of dissolved oxygen in bottom water increases, and the abnormal value of Ce in sediment tend to increase (Wilde et al. 1996). The negative anomaly of Ce is mainly due to the loss or fractionation of Ce during the precipitation of metal oxides, indicative of an anoxic reduction environment, while the positive anomaly of Ce indicates the enrichment of Ce, indicating that the seawater is in an oxidising environment.

The $\delta\text{Ce}_{\text{CN}}$ values of the various lithologies in the black rock series of the two study areas fall 0.39–0.95 and 0.43–1.05, respectively. Except for one value of 1.05, the residual values are all negative anomalies (Table 3), indicating that the study area likely represents a reducing environment at the time of deposition. Eu is a variable valence element with two valence states (Eu^{2+} and Eu^{3+}). Zhao (1993) postulated that the sediments in an active continental margin would be rich in heavy REE, but not

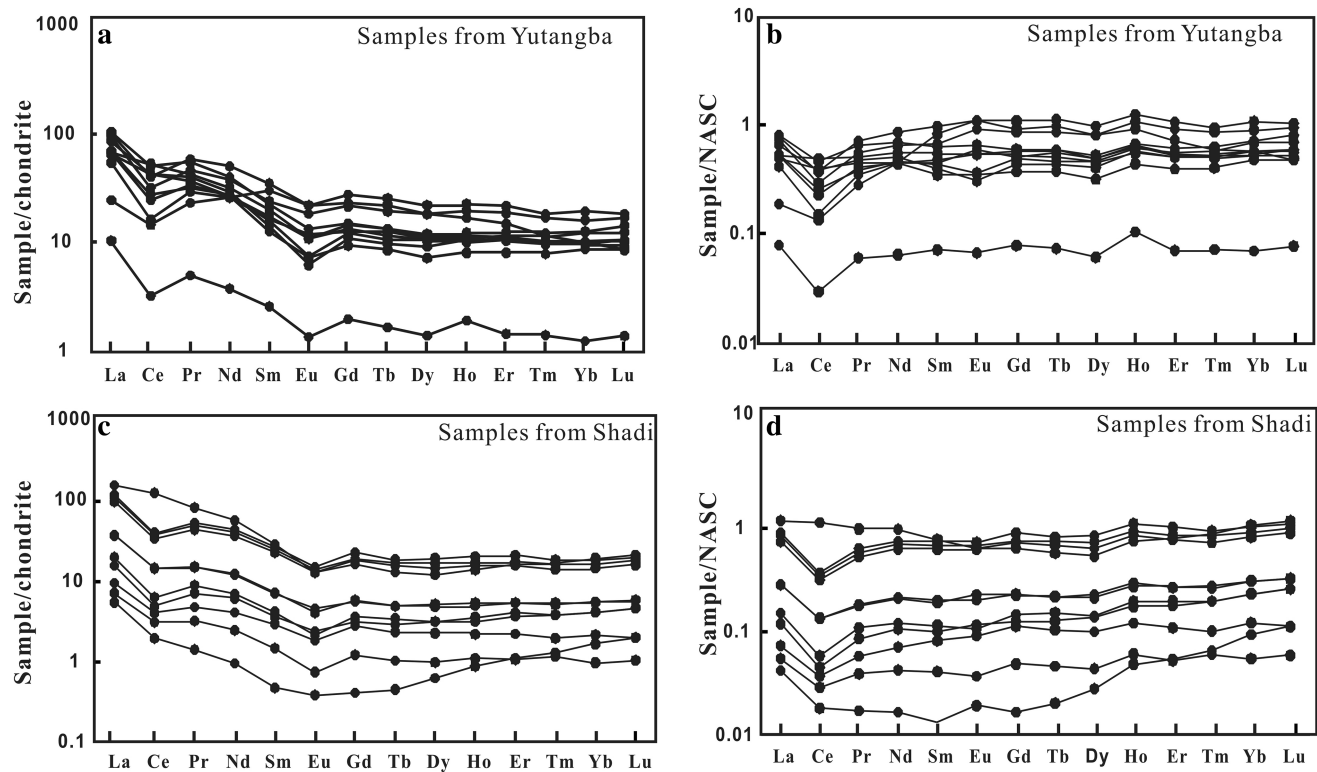


Fig. 4 REE patterns of the Se-rich siliceous rocks in Enshi, Hubei Province **a, c** Chondrite-normalized REE patterns of different study areas (chondrite-normalized values after Sun and McDonough 1989); **b, d** North American Shale-normalized REE patterns of different study areas (North American shale-normalized values after Boynton 1984)

Table 4 Silicon and oxygen isotopic composition (‰) of the siliceous rocks in Enshi, Hubei Province, China

Sample nos	Lithology	$\delta^{18}\text{O}_{\text{V-SMOW}}\text{\textperthousand}$	$\delta^{30}\text{Si}_{\text{NBS-28}}\text{\textperthousand}$	T°C
YTBJ0-1a	Siliceous rock	23.4	0.7	67.1
YTB-5	Siliceous rock	25.4	1.6	55.0
YTB10-14-1	Siliceous rock	25.1	1.5	56.8
YTB-6	Siliceous rock	25.8	1.1	52.8
YTBJ-12a	Siliceous rock	27.3	0.6	44.7
SD10-3	Siliceous rock	25.7	1.3	53.3
SD10-8	Siliceous rock	25.7	0.9	53.3
SD10-9	Siliceous rock	26.3	1	50.0
SD10-14-2	Siliceous rock	26.3	1.2	50.0

display any Eu deficiency, while the sediments formed at a passive continental margin were relatively rich in light REE, and that any δEu would be a negative anomaly. Determined $\delta\text{Eu}_{\text{CN}} = 0.49\text{--}0.83$ and $0.11\text{--}0.17$, $\delta\text{Eu}_{\text{SN}} = 0.79\text{--}1.24$ and $0.82\text{--}1.29$, respectively for the investigated black rock series from the two study areas indicate that δEu in the study area all display a negative anomaly. Moreover, the LREE/HREE ratios for the two study areas

reflect that the black rock deposits likely formed at a passive continental margin.

5.2 Petrogenesis

The ratio of characteristic elements can well reflect the genesis of black rock series. Boström and Peterson (1969) studied high-temperature heat flow sediments near the eastern Pacific Ocean ridge. They believed that the sediments affected by the high-temperature heat flow generally were enriched in Fe and Mn, but lacked Al and Ti, while Al and Ti were deficient. The $\text{Al}/(\text{Al} + \text{Fe} + \text{Mn})$ ratio has become a parameter to help assess the genesis of black rock series. For example, the hydrothermal deposits of the East Pacific Ocean uplift have a value of 0.01, which is identical to those collected in drilling of the deep-sea, $\text{Al}/(\text{Al} + \text{Fe} + \text{Mn}) = 0.01$. The average ratio of hydrothermal siliceous rocks found in Leg32 is 0.12, while that of the Triassic Kamiaso biogenetic semi pelagic siliceous rocks in central Japan is 0.60 (Yamamoto 1987). If the ratio of $\text{Al}/(\text{Al} + \text{Fe} + \text{Mn})$ in marine sediments is less than 0.4, it is likely of hydrothermal origin, while those greater than 0.4, reflects a source with biogenic input (Boström et al. 1973).

The determined $\text{Al}/(\text{Al} + \text{Fe} + \text{Mn})$ ratios of the black rock series from the two study areas display great variation.

Table 5 Sulfur isotopic composition (‰) of pyrites of the siliceous rock in Enshi, Hubei Province, China

Sample nos	Lithology	$\delta^{34}\text{S}_{\text{CDT}}\text{\%}$	Sample nos	Lithology	$\delta^{34}\text{S}_{\text{CDT}}\text{\%}$
YTBZ-4	Pyrite	– 40.18	YTBZ-8	Pyrite	– 49.27
YTBZ-10	Pyrite	– 19.32	YTBZ-1	Pyrite	– 31.30
YTBZ-9	Pyrite	– 20.33	SD10-4	Pyrite	– 23.14
YTBZ-3-1	Pyrite	– 32.43	SD10-5	Pyrite	– 22.83
YTBZ-7	Pyrite	– 29.06	SD10-10	Pyrite	– 23.45
YTBZ-3	Pyrite	– 29.67	SD10-7	Pyrite	– 21.66

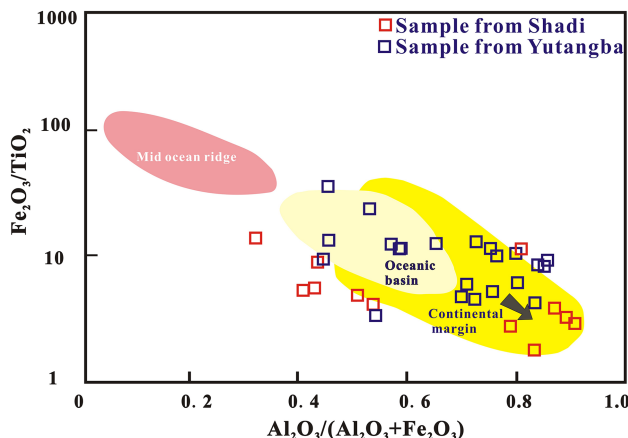


Fig. 5 $\text{Fe}_2\text{O}_3/\text{TiO}_2$ - $\text{Al}_2\text{O}_3/(\text{Al}_2\text{O}_3 + \text{Fe}_2\text{O}_3)$ diagram of the siliceous rocks in Enshi, Hubei Province (Murray 1994)

The values of the siliceous rocks samples collected in the Yutangba mining area fall in 0.19–0.44, which are close to the values of hydrothermal siliceous rocks. In contrast, the values for the other carbonaceous shale samples lie between 0.45 and 0.66. The $\text{Al}/(\text{Al} + \text{Fe} + \text{Mn})$ value of siliceous rock in the black rock series of the Shadi area falls between 0.12 and 0.26, which likely suggests a hydrothermal origin. However, two siliceous rock samples lie in the range of 0.54 and 0.65, while the other samples in Shadi fall in the range of 0.60 and 0.81, which indicates that terrigenous materials were added during the depositional process (Table 1).

Cr is a typical mantle element (Feng et al. 2009), and the content of Cr in the siliceous rocks in two study area is very high (up to 1820 ppm and 308 ppm, respectively, Table 2), suggesting that mantle materials may be involved in the diagenesis of siliceous rocks. Ni and Mo contents are high too (416 and 1314 ppm, which is similar to Lower Cambrian Se-rich siliceous rocks in Zunyi, Guizhou Province.

Se is a kind of nucleophilic element, with an enrichment coefficient of nearly 500 relative to the original abundance of crust. For example, the volcanic sulfur in Bali contains 18% Se, while the volcanic sulfur in Hawaii contains 20% Se. Zheng et al (2006) found that the siliceous of carbonaceous siliceous rocks in the Permian Gufeng Formation in Enshi Prefecture, western Hubei Province came

from volcanic clastic sediments, which were the eruption products of Emeishan basalt in the same period in Southwest China. It can be seen that all kinds of samples have obvious Se enrichment characteristics compared with Se abundance in the crust (Table 2). And Se content is positively correlated with Ni–Mo–V–Cr content (Fig. 3). We think that dispersed element Se enrichment may be the result of many factors (abundant sulfide, hydrothermal sedimentation, and volcanism), which not only leads to the extraordinary enrichment of Ni, Mo, and V, but also causes Se enrichment in siliceous rocks (Feng et al 2004, 2009).

Due to the high deposition rate of hot water depositional systems, which are often enriched in U and the U/Th ratio of hydrothermal sedimentary rocks is larger than 1.0. By contrast, the U/Th of aqueous deposit rocks is < 1.0 (Rona 1978). As mentioned above, the U/Th ratio of the investigated siliceous rocks samples in both study areas is greater than 2.0 (Table 2) and favors that both belonging to a range of hydrothermal sedimentary rocks.

According to the strata studied from the Niutitang Formation in the Hunan and Guizhou Provinces of China (Li and Gao 1995), there are obvious differences in REE composition between marine hot water sediments and normal seawater sediments. Generally, the total amount of REE in marine hot water sediments is relatively low, with clear negative Ce anomalies present. Further, the LREE/HREE ratio is small, and the standardization curve of REE shale in North America is close to horizontal or with a left tilt. On the contrary, the total amount of REE in normal seawater sediment is high, Ce has a positive anomaly, the LREE/HREE ratio is relatively large, and the shale standardization curve of REE in North America has an obvious right tilt phenomenon. The REE curves of the black rocks in the two study areas after shale standardization in North America are close to horizontal or slightly left inclined and both have negative Ce anomalies (Figs. 4b, d), indicating that they have sedimentary characteristics typical of marine hot water solutions.

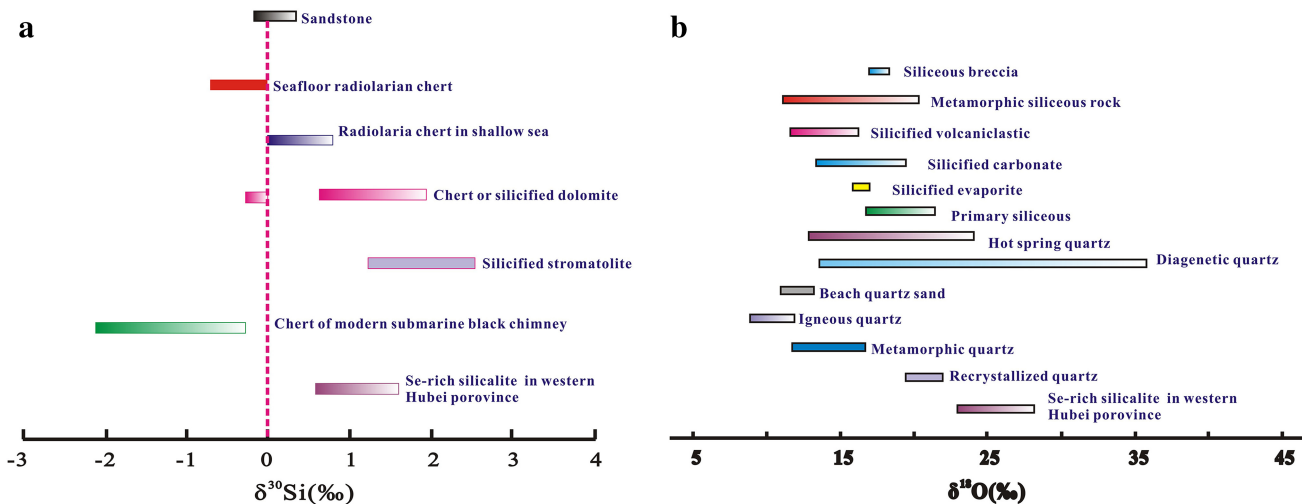


Fig. 6 $\delta^{30}\text{Si}$ (a Douthitt 1982; Clayton 1986; Song and Ding 1989) and $\delta^{18}\text{O}$ (b Alan and Samuel 1970; Knauth and Lowe 1978; Robert and Toshilo 1986; Francois 1988; Peng et al. 1995, 1999) values of siliceous rocks with various genesis

5.3 Evidence from Si-, O-, and S- isotopic studies

5.3.1 Si-isotopes

Si has no valence in nature, mainly occurring in the form of the $[\text{SiO}_4]^{2-}$ tetrahedron, so the kinetic fractionation of Si isotopes is very small, and the change to Si isotopes caused by geological processes thus is not large. Kinetic fractionation of silicon isotopes during SiO_2 precipitation and biological processes in solution at low temperature are the main reasons for any changes to silicon isotopes in nature (Douthitt 1982). It has been shown that the $\delta^{30}\text{Si}$ value of siliceous rocks formed in a shallow marine carbonate environment is generally high (from 1.1‰ to 3.4‰). The $\delta^{30}\text{Si}$ value of siliceous rocks in the deep sea, semi-deep sea, and shallow sea sedimentary environment tend to increase gradually (0.16–0.4–1.3, Song and Ding 1989). The geological age of Se-rich black rock series in the study area is consistent with the concurrent volcanic activity of surrounding rocks (e.g., the eruption of Emeishan basalt) caused by plate extension. This occurred in an extensional geotectonic setting, where the eruption of Emeishan basalt into the seawater rich in siliceous material resulted in a large amount of Se and Mo elements precipitating as the source sediment. In the Late Permian, there was a carbonate platform shallow sea area with a length of more than 240 km and a width of more than 150 km in the southwest of Hubei and the east of Sichuan. The platform depression extended to the Yunyang area of Sichuan in an NW direction (Yu 1993). In the process of migration, ^{28}Si precipitates preferentially relative to ^{30}Si , which makes the $\delta^{30}\text{Si}$ value of dissolved Si in seawater solution increase continuously, and finally it is transported to the shallow sea area of a closed basin, where it begins to settle out of

solution. At this time, the precipitation speed of Si isotopes becomes faster and the dynamic fractionation becomes smaller, leading to the enrichment of ^{30}Si in the precipitating phase. The determined $\delta^{30}\text{Si}$ values of siliceous rocks in the Yutangba area and of the Shadi black rock series are 0.6–1.6‰ and 0.9–1.3‰, respectively (Table 4), which are close to the distribution range of a shallow sea sedimentary environment, and are consistent with the lithofacies paleogeographic environment in the study area mentioned above.

In general, there are different $\delta^{30}\text{Si}$ values in siliceous rocks or quartz reflecting their different types of genesis (Douthitt 1982). The variation range of $\delta^{30}\text{Si}$ value of biogenic siliceous rocks is between –1.1‰ and 1.7‰, while that for authigenic quartz in low-temperature groundwater is between 1.1‰ and 1.4‰. In the case of hydrothermal sedimentary siliceous rocks, $\delta^{30}\text{Si}$ is between –1.5‰ and 0.8‰, and that of secondary quartz is between –0.2‰ and 0.3‰. $\delta^{30}\text{Si}$ for volcanic eruption chemical sedimentary siliceous rocks is between –0.5‰ and –0.4‰, whereas that of modern hot spring siliceous sediments is –0.5‰. The value of $\delta^{30}\text{Si}$ ranges from –3.4‰ to 0.2‰ in deposits of modern hot spring silicon blooms (mainly negative), the value of $\delta^{30}\text{Si}$ is between –0.6‰ and 0.1‰ for deep-sea radioactive siliceous rocks, and between –3.1‰ and 0.4‰ for modern “black chimney” siliceous sediments (Douthitt 1982; Clayton 1986; Song and Ding 1989; Ding 1994). The $\delta^{30}\text{Si}$ values of the siliceous rocks in Yutangba siliceous rocks and Shadi black rock series are 0.6‰–1.6‰ and 0.9‰–1.3‰, respectively (Table 4; Fig. 6a), which are different from those of metasomatic siliceous rock, volcanic eruption chemical sedimentary siliceous rock, but similar to those of chert or silicified dolomite and biogenetic siliceous rock (from

– 1.1‰ to 1.7‰), with a low-temperature affinity for authigenic quartz in groundwater.

The original Si source of the study area is thought to relate to a volcanic eruption, which leads to the enrichment of Si in the seawater. At that time, no siliceous rocks were deposited. At the end of the Permian, a reducing environment formed in a closed basin (Yu 1993). At that time, the flow of the sea-water was restricted into this basin, which favored the accumulation of dead organisms, providing a rich input of organic carbon to that area. Selenium and silicon were thus fixed within a large quantity of carbonaceous sediments, resulting in the formation of selenium-rich black rock series strata in the study areas.

5.3.2 Evidence from O isotopes

The $\delta^{18}\text{O}$ value can be used to help determine the source of quartz, feldspar and other minerals in a certain rock, as the distribution range of $\delta^{18}\text{O}$ values for quartz of differing genesis is dissimilar (Alan and Samuel 1970). For example, the characteristic $\delta^{18}\text{O}$ values of quartz in igneous rocks may range between 8.3‰ and 11.2‰, with an average of 9.0‰; $\delta^{18}\text{O}$ values of metamorphic quartz are commonly in the range 11.2‰ and 16.4‰, with an average of 13‰–14‰; $\delta^{18}\text{O}$ values of hydrothermal quartz, formed at hot springs show a wide range of between 12.2‰ and 23.6‰; as are the $\delta^{18}\text{O}$ values for diagenetic quartz that may range between 13‰ and 36‰, with an average of 22‰; the $\delta^{18}\text{O}$ values of modern beach sand quartz falls in a narrow range of 10.3‰ and 12.5‰, with an average of 12‰. Where quartz has undergone a process of re-crystallization, the $\delta^{18}\text{O}$ values may lie between 19.3‰ and 21.8‰, with an average of 20.45‰ (Fig. 6b; Alan and Samuel 1970; Knauth and Lowe 1978; Robert and Toshilo 1986; Francois 1988; Peng et al. 1995, 1999).

The determined $\delta^{18}\text{O}_{\text{V-SMOW}}$ values of siliceous rocks with different characteristics in the Yutangba mining area and Shadi black rock series span a range of values between 25.0‰ and 27.3‰ (Table 4; Fig. 6b). These $\delta^{18}\text{O}$ values from the samples in the study area are significantly different to those of metasomatic siliceous rocks (from 12.0‰ to 20.3‰, Clayton 1986), but close to the $\delta^{18}\text{O}$ values of possible primary siliceous rocks (from 17.0‰ to 22.1‰, Clayton 1986).

Siliceous rocks are dense and hard; with strong resistance to exchange, and their isotopic composition often is little changed since they were formed. Thus, the oxygen isotopic composition of siliceous rocks can be used to determine their formation temperature (Peng et al. 1995). According to the oxygen isotope equilibrium fractionation equation for chert and seawater 1000 $\ln \alpha_{\text{chert-water}} = 3.09 \times 10^6 \text{ T}^{-2} - 3.29$ (Knauth and Epstein 1976), the formation temperature of chert can be estimated. In the

same way, the oxygen isotope equilibrium fractionation equation of quartz and water 1000 $\ln \alpha_{\text{quartz-water}} = 3.38 \times 10^6 \text{ T}^{-2} - 3.40$, allows for the calculation of the formation temperature of single mineral grains of quartz (Table 4; Clayton et al. 1972). Accordingly, we have determined the temperature range of Yutangba siliceous rock to have formed between 44.7 and 67.1 °C, and that of the materials in the Shadi area to have formed between 53.3 and 55.0 °C. This latter temperature is nearly the same as 56 °C, measured near the vent of hot water at the depths of the Red Sea (Rona 1978). Our determinations indicate that the temperature range of the ancient seawater in the study area spanned a range between 44.7 and 71.8 °C when the siliceous rock formed, suggesting that SiO_2 derived from the hot water.

5.3.3 Evidence from S isotopes

One of the reasons why the black rock series in the Enshi area is famous is that the area is rich in the dispersed element Se. Selenium and the element S both belong to the sixth main group of elements in the periodic table. It has been shown that one of the most important occurrence states of Se in the Yutangba selenium ore is that Se and S co-exist in the ore in an isomorphic relationship (Feng et al. 2004). Hence, the source of S in this area may undoubtedly help to decipher the source of the Se present.

Generally, there are three reservoirs of sulfur in the Earth: (1) mantle-derived sulfur, with isotopic composition of between – 3‰ and 3‰ (Chaussidon and Lorand 1990); (2) Seawater sulfur, with isotopic composition of about 20‰, and (3) Organic (bacterial) reductive/biogenic sulfur under open sedimentary conditions, which exhibits a large negative sulfur isotopic value (Rollinson 1993). The determined values of $\delta^{34}\text{S}_{\text{V-CDT}}$ in the black rock series of Yutangba are between – 49.27‰ and – 19.23‰ (Table 5). The values of $\delta^{34}\text{S}_{\text{V-CDT}}$ in the Shadi area exhibit little variation (from – 23.45‰ and – 21.66‰), however, both show the characteristics related to organic reduction/biogenic.

It is well known that the Permian Triassic period was the key period of Pancontinental formation, subduction, and the demise of the Tethys Ocean, coupled to northward drift of Gondwana and its amalgamation with the ancient land, Lauya (Huang and Chen 1987). From the late Permian to the Early Triassic, the Tethys block moved from $\sim 10^\circ$ north latitude to 30° – 60° north latitude. During this period, the global climate changed from a warm and humid marine climate to a dry and hot continental climate, which was accompanied by large-scale extinction events. The largest transgression event since the Late Paleozoic began in the Late Early Permian in Southwest Hubei Province, which ceased the intermittent advance and retreat pattern of

seawater of the Devonian-Carboniferous periods, and helped to form a carbonate platform and shelf environment; in the Late Permian, the Tungwu movement resulted in one overall uplift of the area, which was rapid and extensive, with a subsequent transgression forming clastic coal-bearing lithofacies, carbonate lithofacies, and siliceous argillaceous rock, in cycles (Zhou and Huang 2010). It can be concluded that the water body in this region, at that time, should be a stagnant, anoxic, and stratified oceanic environment, and one that was accompanied in the atmospheric oxygen level equivalent of between a fifth and a tenth that of the level of modern atmospheric oxygen (Frimmel 2005; Hou et al. 2007). It was precise because of the serious lack of oxygen in the water body that the original ecological environment deteriorated sharply, leading to mass extinction in the early stage of the Late Permian (Wignall 2001).

6 Conclusions

The black rock series in two study areas may have formed in a transitional position between the ocean basin and the continental margin, in the process of sedimentary, more terrigenous clastic materials entered. Two study areas also rich in lithophile elements V and Cr, $\delta\text{U} > 1.0$, U/Th and $\text{V}/(\text{V} + \text{Ni})$ ratio indicate that the Se-rich strata of black rock series in the Enshi areas occurred in an anoxic reducing environment. From Si–O isotope geochemistry, the original Si source of the study area is thought to relate to a volcanic eruption, which leads to the enrichment of Si in the seawater. The determined values of S isotope in the black rock series of two study areas both show the characteristics related to organic reduction/biogenic.

Acknowledgements The research is supported by the General Project of Natural Science Foundation of Shaanxi Province (2020JM-423). We are grateful for the assistance in the Field of Professor Jianming Zhu of China University of Geosciences (Beijing) and Youqiang Qi, an associate researcher of the Institute of Geochemistry, Chinese Academy of Sciences. We also acknowledge the help of the State Key Laboratory of Ore Deposit Geochemistry, Institute of Geochemistry, Chinese Academy of Sciences for assistance with the geochemical work.

References

- Alan DH, Samuel MS (1970) Oxygen-18 studies of recent planktonic foraminifera—comparisons of phenotypes and of test parts. *Science* 170(3953):69–71
- Arthur MA, Sageman BB (1994) Marine shales: depositional mechanism and environments of ancient deposits. *Annu Rev Earth Planet Sci* 22:499–551
- Boström K, Peterson MNA (1969) The origin of aluminum-poor ferromanganese sediments of high heat flow on the East Pacific Rise. *Marine Geol* 7:427–447
- Boström K, Kraemer T, Gartner S (1973) Provenance and accumulation rates of opaline silica, Al, Ti, Fe, Mn, Cu, Ni and Co in Pacific Pelagic sediments. *Chem Geol* 11(2):123–148
- Chaussidon M, Lorand JP (1990) Sulphur isotope composition of orogenic spinel iherzolite massifs from Ariège (North-Eastern Pyrenees, France): an ion microprobe study. *Geochim Cosmochim Acta* 54:2835–2846
- Clayton RN (1986) High temperature isotope effects in the early solar system. *Rev Mineral* 16:129–139
- Clayton RN, Mayeda TK (1963) The use of bromine pentafluoride in the extraction of oxygen from oxide silicates for isotopic analysis. *Geochim Cosmochim Acta* 27:43–52
- Clayton PJ, Halikas JA, Maurice WL (1972) The depression of widowhood. *Br J Psychiatry* 120:71–78
- Dill H (1986) Metallogenesis of Early paleozoic graptolite shales from the Graafenthal Horst (Northern Bavaria-Federal Republic of Germany). *Econ Geol* 81(4):889–903
- Douthitt CB (1982) The geochemistry of the stable isotopes of silicon. *Geochim Cosmochim Acta* 39(5):1179–1186
- Fan HF, Wen HJ, Ling HW, Yu WX (2005) Determination of trace selenium in geological samples by Hydride generation atomic fluorescence spectrometry—a comparative experiment of two different dissolution methods. *Bull Mineral Petrol Geochem* 24(3):200–203 (in Chinese with English abstract)
- Feng CX (2004) The enriching-mechanism of Se of Cambrian and Permian silicalite formation in the peripheral margins of Yangtze Block: taking Yutangba and Ziyang Se-rich areas as an example. Ph. D. Dissertation. Guiyang: Institute of Geochemistry, Chinese Academy of Science (in Chinese with English abstract)
- Feng CX, Liu JJ, Liu S, Hu RZ (2002) The geochemistry and petrogenesis of siliceous rocks of Se diggings in Yutangba. *Acta Sedimentol Sin* 20(4):727–732 (in Chinese with English abstract)
- Feng CX, Liu JJ, Hu RZ, Liu S (2004) Geochemistry of the Yutangba Se deposit in western Hubei Province China. *Chin J Geochem* 23(3):255–264
- Feng CX, Jiajun L, Shen L, Ruizhong H, Guoxiang C (2009) Petrogenesis and sedimentary environment of the cherts from Yutangba, western Hubei Province: evidence from silicon, oxygen, carbon and sulfur isotopic composition. *Acta Petrol Sin* 25(5):1253–1259 (in Chinese with English abstract)
- Francois R (1988) Carbon and oxygen isotope variations in Precambrian cherts. *Geochem Cosmochim Acta* 52(6):1473–1478
- Frimmel HE (2005) Archean atmospheric evolution: evidence from the Witwatersrand gold fields, South Africa. *Earth Sci Rev* 70:1–46
- Girty GH, Rdige DL, Knaack C, Johnson D, Al-Riyami RK (1996) Provenance and depositional setting of Paleozoic chert and argillite, Sierra Nevada California. *J Sediment Res* 66(1):107–118
- Hubei Provincial Bureau of Geology and Mineral Resources (1990) Hubei Provincial Regional Geology-Special Geological Report of the Ministry of Geology and Mineral Resources of the People's Republic of China, I. Regional Geology No. 20. Geological Publishing House, pp 1–644
- Hou KJ, Li YH, Wan DF (2007) Constraints on the Archean atmospheric oxygen and sulfur cycle from mass-independent sulfur records from Anshan-Benxi BIFs, Liaoning province China. *Sci China (Series D)* 50(10):1471–1478
- Huang JQ, Chen BW (1987) The evolution of the Tethys in China and adjacent regions. Geological Publishing House, Beijing, pp 1–109 (in Chinese)

- Jiang SY, Zhao HX, Cheng YQ, Yang T, Tang JH, Ling HF (2007) Trace and rare earth element geochemistry of phosphate nodules from the lower Cambrian black shale sequence in the Mufu mountain of Nanjing, Jiangsu Province China. *Chem Geol* 244(3–4):584–604
- Jones B, Manning DAC (1994) Comparison of geochemical indices used for the interpretation of paleoredox conditions in ancient mudstones. *Chem Geol* 111:111–129
- Knauth LP, Epstein S (1976) Hydrogen and oxygen isotope ratios in nodular and bedded cherts. *Geochem Cosmochim Acta* 40(9):1095–1108
- Knauth LP, Lowe DR (1978) Oxygen isotope geochemistry of cherts from the Onverwacht Group (3.4 billion years), Transvaal, south Africa, with implications for secular variations in the isotopic composition of cherts. *Earth Planet Science Lett* 41(2):209–222
- Li SR, Gao ZM (1995) REE characteristic of black series of the lower Cambrian Niutitang formation in Hunan-Guizhou provinces, China—with a discussion on the REE patterns in marine hydrothermal sediments. *Acta Mineral Sin* 15(2):225–322 (**in Chinese with English abstract**)
- Liu JJ, Feng CX, Li ZM, Wang JP, Liu SR, Zhou GF (2005) The research of significance and discovery of Secondary native selenium in the Yutangba Se deposit, western Hubei. *Geosciences* 19(4):531–537 (**in Chinese with English abstract**)
- Liu JJ, Cao Y, Carranza EJM, Feng CX, Zhai DG, Wang JP, Li JX (2014) Characterization of secondary native selenium in the Yutangba Se Deposit, western Hubei. *China Resour Geol* 64(3):271–281
- Murray RW (1994) Chemical criteria to identify the depositional environment of chert: general principles and application. *Sed Geol* 90(3–4):213–232
- Murray RW, Ten Brink MRB, Jone DL, Gerlach DC, RussIII GP (1990) Rare earth elements as indicators of different marine depositional environments of chert and shale. *Geology* 18(3):268–271
- Niu ZJ, Xu AW, Duan QF, Fu TA (2000) Original and enrichment of Se in Permian strata in the north part of Jianshi Hubei. *Reg Geol China* 19(4):396–401 (**in Chinese with English abstract**)
- Peng J, Xia WJ, Yi HS (1995) Silicon and oxygen isotopic compositions and origin analysis of Late Precambrian bedded cherts in western Hunan. *Geol Rev* 41(1):34–41 (**in Chinese with English abstract**)
- Peng J, Xia WJ, Yi HS (1999) Geochemical characteristics and depositional environments of the Late Precambrian environments of the Late Precambrian bedded siliceous rocks in western Hunan. *Sediment Facies Palaeogeogr* 19(2):29–37 (**in Chinese with English abstract**)
- Qi L, Hu J, Gregoire DC (2000) Determination of trace elements in granites by inductively coupled plasma mass spectrometry. *Talanta* 51(3):507–513
- Rimmer SM (2004) Geochemical paleoredox indicators in Devonian-Mississippian black shales, central Appalachian Basin (USA). *Chem Geol* 206:373–391
- Robert NC, Toshilo KM (1986) Oxygen isotopes in Shergotty (in Shergotty Consortium and SNC meteorites). *Geochim Cosmochim Acta* 50(6):979–982
- Rollinson HR (1993) Using geochemical data: evaluation presentation and interpretation. Longman, Harlow, p 352
- Rona PA (1978) Criteria for recognition of hydrothermal mineral deposits in ocean crust. *Econ Geol* 73:135–160
- Shi XB, Wong MZ, Luo H, Xu LL, Gong ZY, Zhao XS, Duan XF (2016) Sequence stratigraphy of Middle Permian Gufeng formation from Se-rich area in Enshi, Southwestern Hubei. *Geol Miner Resour South China* 32(1):1–9
- Song TR, Ding TP (1989) The trying application of silicon isotope of silication to analyzing sedimentary faces. *Chin Sci Bull* 34(18):1408–1411 (**in Chinese**)
- Sugisaki R, Yamamoto K, Adachi M (1982) Triassic bedded cherts in central Japan are not pelagic. *Nature* 298:644–647
- Sun SS, McDonough W (1989) Chemical and isotopic-systematics of oceanic basalts: implication for Inantie composition and processes. In: Saunders AI, Norry MJ (eds) Magmatism in ocean basins. Geological Society London, Special Publications, London, vol 42, pp 313–345
- Tian SP, Zhu YN, Wang QL, Zhu HJ (2007) The metallogenetic condition and its prognosis of Se deposit in east Enshi state of Hubei Province. *Geol Chem Miner* 39(3):141–149 (**in Chinese with English abstract**)
- Tiping D, Shaoyong J, Defang W, Li YH, Li JC, Song HB, Liu ZJ, Yao XM (1994) Silicon isotopic geochemistry. Geological Publishing House, Beijing, pp 1–102
- Tong Li (1992) The Statistical characteristics of the abundance of chemical elements in the earth's crust. *Geol Prospect* 28(10):1–7 (**in Chinese with English abstract**)
- Wignall PB (1994) Black shales. Oxford University Press, Oxford
- Wignall PB (2001) Large igneous provinces and mass extinctions. *Earth Sci Rev* 53(1–2):1–33
- Wilde SA, Middleton MF, Evans BJ (1996) Terrane accretion in the southwestern Yilgarn Craton: evidence from a deep seismic crustal profile. *Precambr Res* 78:179–196
- Yamamoto K (1987) Geochemical characteristics and depositional environments of cherts and associated rocks in the Franciscan and Shimanto terranes. *Sed Geol* 52:65–108
- Yao LB (2002) Geochemical characteristics and genesis of Yutangba Selenium Deposit. PhD thesis of Institute Geochimstry, Chinese Academy of Sciences (in Chinese)
- Yao LB, Gao ZM, Yang ZS, Long HB (2002) Genesis of selenium rich siliceous rocks in Yutangba Selenium Deposit. *Sci China* 32(10):54–63 (**in Chinese**)
- Yu RY (1993) Preliminary analysis on the geological characteristics and origin of the Shuanghe Se ore beds Hubei Hubei. *Geology* 7(1):50–56 (**in Chinese with English abstract**)
- Yu T, Yang ZF, Wang R, Zeng QL, Hou WL (2018) Characteristics and sources of soil Se and other elements in typical high Se soil area of Enshi. *Soil* 50(6):1119–1125 (**in Chinese with English abstract**)
- Zhao ZH (1993) Controlling factors of geochemical characteristics of Eu. *J Nanjing Univ (Geoscience)* 5(3):271–280 (**in Chinese with English abstract**)
- Zheng X, Qian HD, Wu XM (2006) Geochemical and genetic characteristics of Se ore deposit in Shuanghe, Enshi Hubei Province. *Geol China Univ* 12(1):83–92 (**in Chinese with English abstract**)
- Zhou SQ, Huang GZ (2010) Characteristics and geostructure significance of the late Permian intracontinental Chasmic basin in southwest of Hubei. *Resour Environ Eng* 24(2):130–133 (**in Chinese with English abstract**)